nature physics

Article

https://doi.org/10.1038/s41567-022-01895-3

Coherent backscattering of entangled photon pairs

Received: 5 May 2022

Accepted: 25 November 2022

Published online: 23 January 2023



Mamoon Safadi¹, Ohad Lib **1**, Ho-Chun Lin **1**, Chia Wei Hsu **1**, Arthur Goetschy³ & Yaron Bromberg **1**. ⊠

Correlations between entangled photons are a key ingredient for testing fundamental aspects of quantum mechanics and an invaluable resource for quantum technologies. However, scattering from a dynamic medium typically scrambles and averages out such correlations. Here we show that multiply scattered entangled photons reflected from a dynamic complex medium remain partially correlated. In experiments and full-wave simulations we observe enhanced correlations, within an angular range determined by the transport mean free path, which prevail over disorder averaging. Theoretical analysis reveals that this enhancement arises from the interference between scattering trajectories, in which the photons leave the sample and are then virtually reinjected back into it. These paths are the quantum counterpart of the paths that lead to the coherent backscattering of classical light. This work points to opportunities for entanglement transport despite dynamic multiple scattering in complex systems.

Entangled photons exhibit correlations that cannot be explained by classical physics. Over the past decades, physicists harnessed entangled states of photons to test some of the most peculiar predictions of quantum mechanics, such as the violation of Bell's inequalities¹ and teleportation². Entangled photons have also proven to be indispensable for quantum technologies, such as device-independent quantum communication³ and linear optical quantum computation⁴. While such states are indeed an invaluable resource, they are typically prone to a variety of processes that affect their non-classical correlations. One ubiquitous and often inevitable process is light scattering from inhomogeneities. Thus, it is crucial to understand how such scattering events affect entangled photons, especially given recent rapid advances in utilizing quantum states of light in real-life scenarios, such as satellite-based entanglement distribution through turbulent atmosphere⁵ and quantum imaging through biological tissue⁶. While entanglement can survive multiple scattering from a static medium if all output modes are accessible 7,8, the dynamic movement of the scatterers constantly changes the state of the photons, washing out correlations in disorder-averaged states $^{9-12}$. In the classical regime, researchers have observed the existence of several so-called mesoscopic phenomena that survive the dynamic movement and disorder averaging I^{3-16} , such as long-range correlations $I^{7,18}$ and coherent backscattering (CBS) I^{9-22} . Thus, it is invaluable to study whether the quantum counterpart of such phenomena can exhibit correlations that are robust to disorder averaging.

Studying quantum states of multiply scattered light poses remarkable theoretical, numerical and experimental challenges, due to the huge Hilbert space spanned by multiphoton states that occupy numerous spatial modes. To circumvent this issue, analogies of multiple scattering were studied in one-dimensional arrays of coupled single-mode waveguides, with engineered and propagation-invariant disorder. Such arrays mimic quantum walks in disordered potentials, which exhibit transverse Anderson localization of photon pairs ^{23–25}. However, experiments in such one-dimensional arrays do not account for the angular degrees of freedom and cannot probe mesoscopic phenomena, such as CBS, universal conductance fluctuations and universal optimal transmission. While theoretical studies indicate that the scattering of quantum states by volumetric disordered samples can exhibit diverse mesoscopic effects in the angle-resolved photon correlations ^{7,26–29}, such features could not be measured in experiments due to the low

¹Racah Institute of Physics, The Hebrew University of Jerusalem, Jerusalem, Israel. ²Ming Hsieh Department of Electrical and Computer Engineering, University of Southern California, Los Angeles, CA, USA. ³ESPCI Paris, PSL University, CNRS, Institut Langevin, Paris, France. —e-mail: yaron.bromberg@mail.huji.ac.il

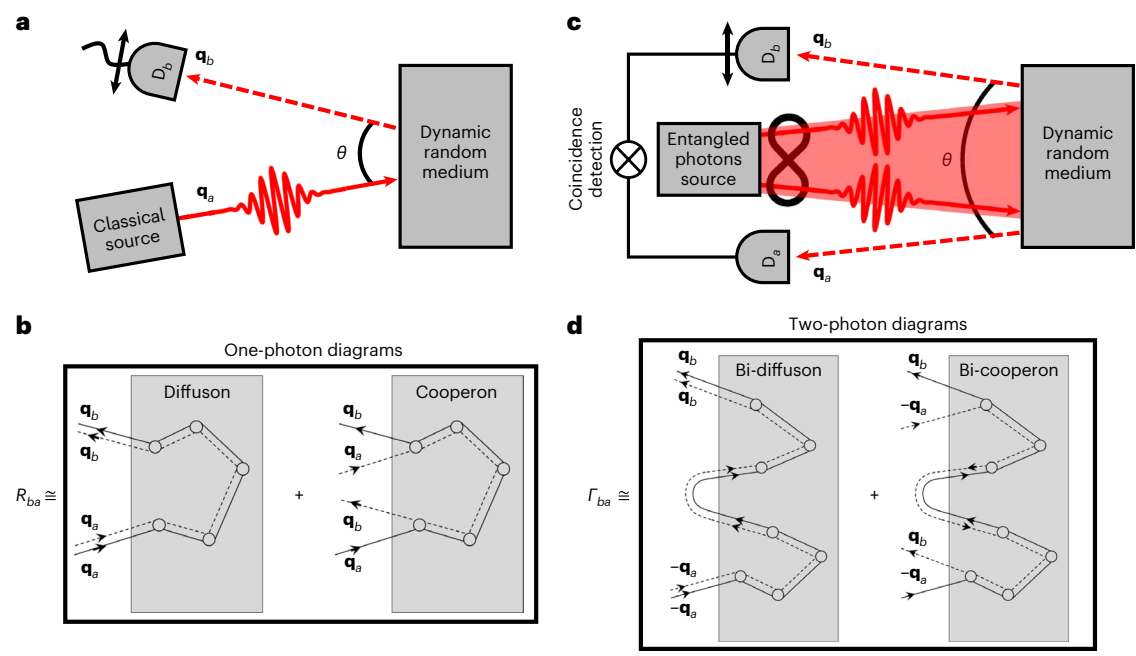


Fig. 1| **Classical and quantum coherent backscattering. a**, Typical experimental scheme of a classical coherent backscattering experiment. A classical coherent plane wave impinges onto a random medium, and the reflected light is collected by a detector (D_b) . At the precise backscattering angle, $\theta = 0^\circ$, an enhancement of the light is observed, the CBS. **b**, Classical CBS diagrams of the mean reflection coefficient R_{bo} , where a (b) represents the input (output) mode with transverse momentum $\mathbf{q}_a(\mathbf{q}_b)$. The first term, the 'diffuson', is an incoherent summation of all path pairings inside the medium. The second term, the 'cooperon', contains all path pairings that visit the same scatterers but in a reversed manner. **c**, Schematic layout of a 2p-CBS experiment. A flux of

entangled photon pairs illuminates the random medium and the backscattered photons with transverse momenta \mathbf{q}_a and \mathbf{q}_b are collected using two detectors whose coincidence events are registered. Here, θ is the angle between the two output modes. \mathbf{d} , The leading diagrams found for 2p-CBS when calculating the two-photon correlation function Γ_{ba} of the two output modes a and b. In Klyshko's advanced wave picture, the detected mode a is replaced by an illumination mode that backpropagates through the system with an opposite transverse momentum $(-\mathbf{q}_a)$, and is detected in mode b. We call these diagrams the bi-diffuson (first term) and bi-cooperon (second term), and they represent the two-photon generalizations of their classical counterparts (see text for more details).

collection efficiency of multiply scattered photons. Experiments in this regime focused instead on global features of the total reflection or transmission that do not resolve the angles $^{30-33}$. Speckles in the angle-resolved two-photon correlations, coined two-photon speckle, were measured only for thin, forward-scattering diffusers, but no meso-scopic correlations were reported $^{34-37}$. Therefore, mesoscopic features of quantum light in high dimensions have not been observed so far.

In this work, we experimentally and theoretically study quantum correlations between pairs of entangled photons that backscatter from a dynamic disordered sample. We discover that even after disorder averaging, the photon pairs remain correlated, revealing a mesoscopic feature of two-photon speckle, which we coin 'two-photon coherent backscattering' (2p-CBS). We succeeded in collecting enough photons to observe a pronounced signal by designing a scattering sample made of a thin rotating diffuser followed by a mirror that reflects the photons back through it. This double-passage configuration allows each photon to scatter twice from the same thin and forward-scattering diffuser, enabling the formation of reciprocal paths, which is a key ingredient for observing coherent backscattering in disordered media. We also perform a theoretical and numerical study in a true multiple-scattering medium to identify the fundamental scattering processes at the origin of the 2p-CBS. Our analysis reveals that the experimentally observed correlations are universal and not unique to the double-passage configuration considered in the experiment. Finally, we show that one can achieve a better estimation of the transport mean free path using 2p-CBS compared to classical CBS.

When a classical plane wave illuminates a disordered medium, a twofold enhancement of the backscattered intensity is observed in the direction opposite to the incoming wave ($\theta = 0^{\circ}$ in Fig. 1a). This region of enhanced intensity, coined the CBS cone, is revealed only

after ensemble averaging over realizations of the disorder, as a single realization is dominated by a strongly fluctuating speckle. Classical CBS has been studied by scattering laser light off a wide array of disordered samples, including powder suspensions¹⁹⁻²², random phase screens³⁸⁻⁴⁰, amplifying random media⁴¹, biological tissues⁴², human bones⁴³, multimode fibres⁴⁴, ultracold atom gases⁴⁵ and liquid crystals⁴⁶, CBS was also observed for other types of classical light, such as pseudothermal⁴⁷ and Raman light⁴⁸, as well as for other types of waves, such as acoustic⁴⁹, seismic⁵⁰ and quantum matter waves⁵¹. The universality and robustness of CBS arises from the optical reciprocity principle⁵², as revealed by a diagrammatic decomposition of the field over the scattering paths, featuring two dominant terms of the reflected intensity²². The first term, the 'diffuson', accounts for a homogeneous background and corresponds to all pairs of paths propagating through the same scatterers identically. The second term, the 'cooperon', accounts for the enhancement observed in the backscattering direction and corresponds to constructive interference of all path pairs propagating through the same scatterers but in a reversed order (Fig. 1b).

The question of whether entangled photon pairs also exhibit coherent backscattering has not been addressed so far. Quantum interference of photon pairs is probed by measuring the rate of coincidence events, namely simultaneous detection of two photons by two single-photon detectors (Fig. 1c). A convenient interpretation of such a detection scheme is provided via Klyshko's advanced wave picture ⁵³, in which the joint two-photon probability of detecting a photon in mode a and a photon in mode b is mapped to the probability of a photon launched into the system from mode a and detected in mode b, after traversing the optical system twice ⁵⁴. Using this representation and a rigorous diagrammatic expansion, we will show (see discussion and Supplementary Sections 4 and 6) that two-photon interference of

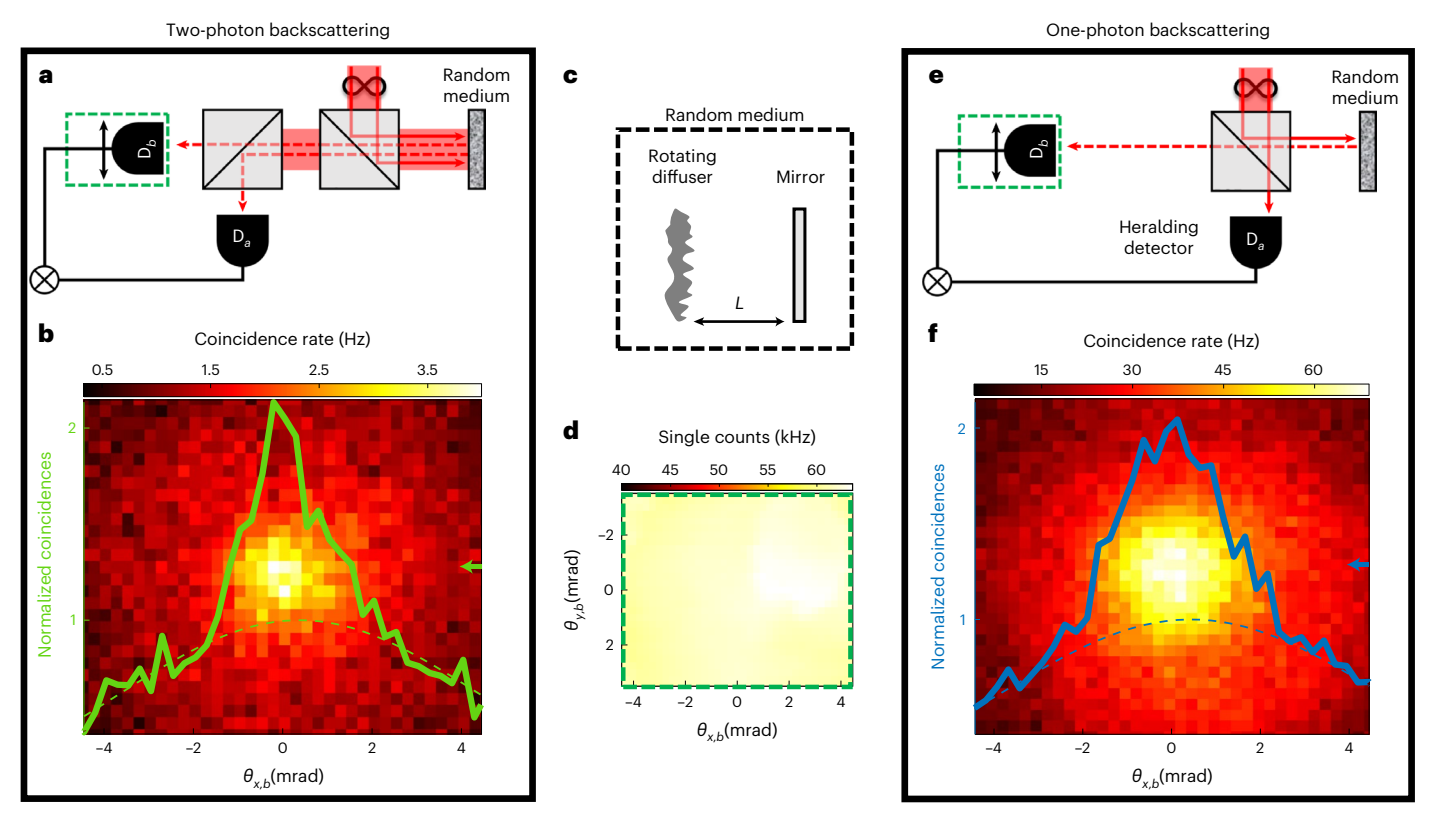


Fig. 2 | **Experimental observation of two-photon and one-photon coherent backscattering. a**, Scheme of the 2p-CBS experiment where entangled photon pairs illuminate the random sample. The backscattered photons are measured via coincidence logic of detectors D_a and D_b , **b**, The two-dimensional coincidence map observed and a normalized cross-section along the indicated row (green arrow). The coincidence distribution exhibits a clear enhancement in the backscattering direction. **c**, The random sample consists of a rotating diffuser and a plane mirror placed behind it at a distance L. **d**, The single counts registered by the scanning detector D_b exhibit a homogeneous distribution over the scanned region. **e**, Scheme of the 1p-CBS experiment, which mimics classical CBS. Heralded single-photon illumination is obtained by a coincidence logic between detector D_b and detector D_a , which is now placed before the random sample. **f**, The two-dimensional coincidence map observed and a normalized cross-section along the

indicated row (blue arrow). Once again, the coincidence distribution exhibits a clear enhancement in the backscattering direction. Despite the diffuser–mirror spacing being the same (L=2.5 cm), the 2p-CBS shape is narrower than the 1p-CBS shape. Both experiments are performed at the far-field plane of the random medium. The transverse momenta of the coincidence counts, as well as the single-counts distribution are expressed in terms of angles $\theta_{x,b} = q_{x,b}/k$, where $\theta_{x,b}$ is the angular position of the scanning detector (D_b) and k is the photon wavenumber (the same goes for $\theta_{y,b}$). The angular location of the static detector (D_a) θ_a was along the optical axis ($\theta_a=0$), such that the background and CBS cones are concentric. The dashed lines in panels ${\bf b}$ and ${\bf f}$ indicate the background fit for each of the 2p-CBS and 1p-CBS experiments on which we perform the normalization. More details about the setup and the fitting procedure are given in the Methods and Supplementary Sections 1 and 5.

the backscattered light does not vanish after disorder averaging and is governed by two new leading diagrammatic terms. The first term, which we coin the 'bi-diffuson', corresponds to all path pairs that visit the same scatterers inside the medium, leave it and are virtually reinjected into it once more, undergoing another scattering sequence. The second term, which we coin the 'bi-cooperon', contains all the path pairs that visit the same scatterers in the first and second passages but in a reversed order (see Fig. 1d).

To experimentally study the backscattering of entangled photons, we illuminate the rotating random sample with a stream of spatially entangled photon pairs generated by spontaneous parametric down conversion (SPDC) (Fig. 2a and Supplementary Fig. 1). The photon pairs are generated at the same wavelength of λ = 808 nm and the same polarization (see Methods for more details). In the thin crystal regime⁵⁴, the SPDC photons are maximally entangled in their spatial degree of freedom (see Supplementary Section 2) and can be described by an Einstein–Podolsky–Rosen (EPR) state $|\psi\rangle = \frac{1}{\sqrt{2N}} \sum_{i=1}^{N} \hat{c}_{\mathbf{q}_i}^{\dagger} \hat{c}_{-\mathbf{q}_i}^{\dagger} |0\rangle$, where N is the number of modes illuminating the random sample and $\hat{c}_{\mathbf{q}_i}^{\dagger}$ is the creation operator of an incident mode with transverse momentum \mathbf{q}_i . We then measure the disorder-averaged coincidence rate between detectors D_a and D_b , placed at the far field of the rotating sample (Fig. 2a). The temporal coincidence window used to register

simultaneous arrival of photons to the detectors is chosen to be 800 ps, much shorter than the average separation time between detected pairs (a few μs). To overcome the challenge of low collection efficiencies of photons backscattered from multiple-scattering samples, we implement the double-passage configuration using a thin diffuser with a scattering angle of $\theta_0 \approx 4.4$ mrad, and a mirror at a distance L behind it (Fig. 2c). This choice of random medium allows us to achieve a collection efficiency of near unity using low numerical aperture lenses (NA \approx 0.1), relaxing the need to use high NA objectives that introduce multiple backreflections, which typically overwhelm the CBS effect.

The coincidence map of detectors D_a and D_b reveals a sharp peak on top of a wide background, with a peak-to-background ratio of approximately 2 (Fig. 2b), which we refer to as 2p-CBS. In contrast, the spatial distribution of the photons detected by the single counts of D_b reveals no discernible structure (Fig. 2d). The fact that the backscattering enhancement is observed only in the two-photon correlation map and not in the single-counts distribution is a hallmark of two-photon interference, distinguishing it from classical CBS. Registering only the single counts of the photons arriving at detector D_b corresponds to tracing out the angular degree of freedom of their twin photons arriving at detector D_a , which results in a mixed state that cannot exhibit single-photon interference³⁴. We note that to obtain a prominent enhancement of the

non-classical light, one has to surpass the two main noise sources in the experiment: the speckle noise of the disorder and the Poisson noise of the coincidence events. To surpass the Poisson noise, we integrated each pixel in the coincidence map for over 200 seconds to accumulate hundreds of coincidence events per pixel. To surpass the speckle noise, the diffuser was rotated and translated in the transverse direction, covering its entire surface, during the acquisition time. In this way, we were able to achieve a sufficient signal-to-noise ratio and observe a pronounced peak of the backscattered quantum light.

We now compare the features of the 2p-CBS shape to the classical CBS shape. Since the flux of classical light is identical to that obtained by repeatedly illuminating the sample with a stream of single photons, classical CBS is identical to the CBS obtained using a single-photon source EBS. Here, we use heralded single photons to measure the classical CBS, referred to as 1p-CBS, by placing the static detector D_a before the scattering sample (Fig. 2e). Now, detection of a photon by detector D_a heralds the presence of its twin and collapses its state to a photon in a plane-wave mode with a well-defined transverse momentum, which illuminates the rotating sample. This backscattered photon is then collected with detector D_b , and its coincidence counts with detector D_a are recorded. Figure 2f depicts the observed 1p-CBS coincidence map, which is clearly wider than the 2p-CBS one.

To investigate the structure of the enhanced region in 2p-CBS, we calculate the two-photon correlation function, Γ_{ba} , defined as

$$\Gamma_{ba} = \overline{\langle \psi | : \hat{n}_{\mathbf{q}_a} \hat{n}_{\mathbf{q}_b} : | \psi \rangle},\tag{1}$$

where $\hat{n}_{\mathbf{q}} = \hat{d}_{\mathbf{q}}^{\dagger} \hat{d}_{\mathbf{q}}$ is the photon number operator of a reflected mode with transverse momentum \mathbf{q} and $\hat{d}_{\mathbf{q}}^{\dagger} (\hat{d}_{\mathbf{q}})$ being the corresponding creation (annihilation) operator, : (...): stands for normal ordering, and ... represents ensemble averaging over different realizations of disorder. This correlation function is proportional to the coincidence rate of two detectors measuring photons reflected by the sample with transverse momenta \mathbf{q}_a and \mathbf{q}_b (see Supplementary Section 3). The operators of the incoming and outgoing modes are related through the reflection matrix r of the sample, as $\hat{d}_{\mathbf{q}_a} = \sum_{a'} r_{\mathbf{q}_a, \mathbf{q}_{a'}} \hat{c}_{\mathbf{q}_{a'}}$, Inserting the reflection matrix and the EPR state into equation (1), we obtain

$$\Gamma_{ba} = \frac{2}{N} \overline{\left|\sum_{i} r_{\mathbf{q}_{b}, \mathbf{q}_{i}} r_{\mathbf{q}_{a}, -\mathbf{q}_{i}}\right|^{2}} = \frac{2}{N} \overline{\left|\left(r^{2}\right)_{\mathbf{q}_{b}, -\mathbf{q}_{a}}\right|^{2}},$$
 (2)

where in the second equality we used optical reciprocity $r_{\mathbf{q},\mathbf{q}'} = r_{-\mathbf{q}',-\mathbf{q}}$ to express Γ_{ba} by the matrix product r^2 .

The 2p-CBS can now be computed by decomposing r^2 over the scattering paths. Modelling scattering by the thin diffuser as Gaussian random processes, we find that in the limit of large diffuser–mirror spacing, $kL\theta_0^2\gg 1$ ($k=2\pi/\lambda$ being the photon wavenumber), Γ_{ba} is dominated by (Supplementary Section 4)

$$\Gamma_{ba} \propto \left\{ 1 + \exp\left[-\frac{(2L\theta_0)^2}{2} (\mathbf{q}_a - \mathbf{q}_b)^2 \right] \right\} \times \exp\left[-\frac{(\mathbf{q}_a + \mathbf{q}_b)^2}{4k^2\theta_0^2} \right]. \tag{3}$$

The first term in the curly brackets can be interpreted as the bi-diffuson (the background) while the second can be interpreted as the bi-cooperon (the 2p-CBS peak). Since the scattering is anisotropic, an envelope representing the finite scattering angle of the diffuser multiplies both terms. The envelope is centred at the same position as the peak of the coincidence map in the absence of scattering, $\mathbf{q}_a + \mathbf{q}_b = 0$, reflecting the fact that scattering broadens the tight momentum anticorrelations of the EPR state. In contrast, the 2p-CBS peak is centred at $\mathbf{q}_a - \mathbf{q}_b = 0$, revealing that after backscattering the photons tend to have correlated transverse momenta. To illustrate the transition from anticorrelated to correlated momentum, we compare in Supplementary Fig. 6 the positions of the experimentally measured coincidence peaks, with and without scattering.

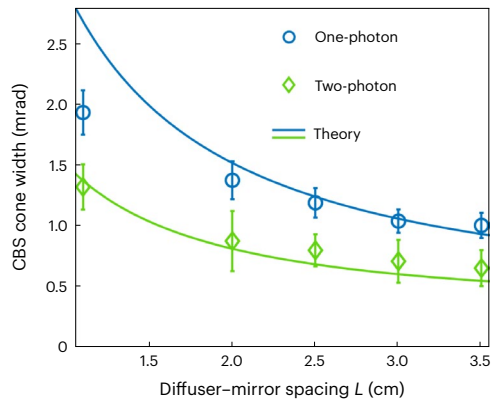


Fig. 3 | **2p-CBS** and **1p-CBS** widths against the diffuser–mirror spacing *L*. The experimentally measured CBS widths of the 2p-CBS are in green diamonds and of the 1p-CBS in blue circles. Solid green line corresponds to the predicted width for 2p-CBS $\Delta\theta_{2p} = \sqrt{\delta_{2p}^2 + (2kL\theta_0)^{-2}}$, where $\delta_{2p}^2 = 2\sigma^2/f_4^2$ accounts for the angular resolution in the 2p-CBS experiment, determined by the radius of the fibre-coupled detectors (σ = 50 µm) and the focal length of the far-field lens (f_4 = 200 mm). Solid blue line corresponds to the theoretically predicted 1p-CBS width, $\Delta\theta_{1p} = \sqrt{\delta_{1p}^2 + (kL\theta_0)^{-2}}$, where $\delta_{1p}^2 = \sigma^2/f_1^2 + \sigma^2/f_4^2$ is the angular resolution in the 1p-CBS experiment, determined by the divergence of the heralding single photon, located at the far field of the crystal (f_1 = 150 mm), and the angular resolution of the fibre-coupled detector. The CBS width extracted at each diffuse–mirror spacing was recorded at over 500 realizations of disorder. Error bars indicate the confidence intervals (95%) of the fit parameter for the CBS width (±the variation in that parameter). See Supplementary Section 4 for more information.

The 1p-CBS, meanwhile, is given by (Supplementary Section 4):

$$R_{ba} \propto \left\{ 1 + \exp\left[-\frac{\left(L\theta_0\right)^2}{2} (\mathbf{q}_a + \mathbf{q}_b)^2 \right] \right\} \times \exp\left[-\frac{\left(\mathbf{q}_a - \mathbf{q}_b\right)^2}{2k^2 \theta_0^2} \right]. \tag{4}$$

 R_{ba} is the mean reflection coefficient that represents the intensity scattered from mode \mathbf{q}_a to mode \mathbf{q}_b , where the first term in the brackets represents the background that corresponds to the diffuson, and the second term represents the CBS shape and corresponds to the cooperon. Once again, an envelope term accounting for the finite scattering angle of the diffuser multiplies both terms. We note that in equation (4) the peak is centred around $\mathbf{q}_a + \mathbf{q}_b = 0$, since in 1p-CBS \mathbf{q}_a marks the transverse momentum of the photon illuminating the sample (Fig. 1a), while in 2p-CBS it marks the transverse momentum of the detected photon (Fig. 1c).

We then measured the 2p-CBS and 1p-CBS angular widths as a function of the diffuser–mirror spacing L. The experimental widths depicted in Fig. 3 (green diamonds for 2p-CBS and blue circles for 1p-CBS) agree with the theoretical curves (solid curves). At small distances, deviations become more apparent and we attribute this to the CBS profile being washed out by the finite background. In Supplementary Section 5 we provide a detailed description of the measuring process and fitting procedure. We note that as the angular widths of the 2p-CBS and 1p-CBS shapes scale as $(2kL\theta_0)^{-1}$ and $(kL\theta_0)^{-1}$, respectively, this signifies that the shape of the 2p-CBS corresponds to the shape of the 1p-CBS yet with a two times larger wavenumber. Interestingly, this unique feature of entangled photons mimicking single photons at double the wavenumber–a quantum feature of entangled photons that often leads to super-resolution and super-sensitivity 56 appears to survive scattering and disorder averaging.

We now address the important question of the universality of the 2p-CBS. Is this phenomenon restricted to the double-passage

One-photon

Two-photon

 $(k\ell)^{-1}$ fits

80

100

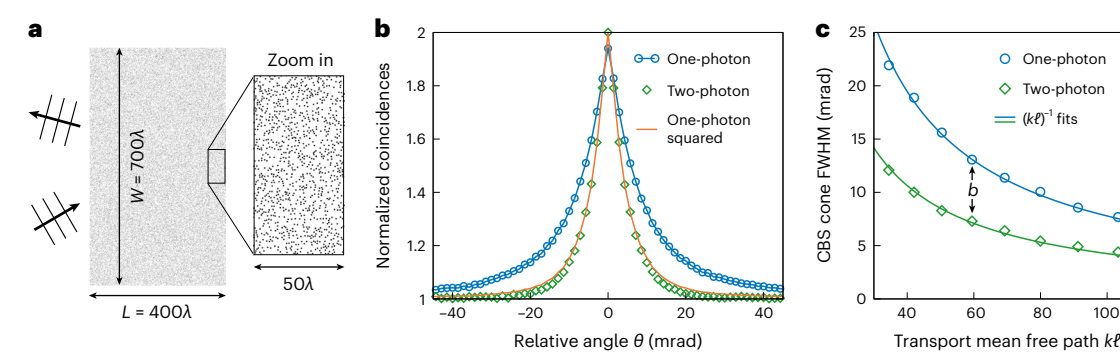


Fig. 4 | Two-photon coherent backscattering from disordered samples in **multiple-scattering regime. a**, Relative permittivity profile $\varepsilon_r(x, y)$ for one realization of disorder. b, Normalized one-photon and two-photon coincidence rates in reflection, R_{ba}/R_0 in blue circles, Γ_{ba}/Γ_0 in green diamonds and

 $1 + [(R_{ha}/R_0) - 0.94]^2$ in orange solid line. The relative angle θ is as labelled in Fig. 1a,c: $\theta = (q_a + q_b)/k$ for 1p-CBS, $\theta = (q_a - q_b)/k$ for 2p-CBS. **c**, The FWHM of the one-photon and two-photon CBS cones. Symbols are numerical data, and solid lines are $0.78/(k\ell)$ and $0.43/(k\ell)$.

configuration and washed out in the presence of strong multiple scattering, or is it robust against any type and strength of disorder? To answer this question, we consider the propagation of entangled photons in opaque disordered media deep in the multiple-scattering regime. In such systems, light experiences, on average, a random walk, and the number of scattering paths contributing to the two-photon correlation function equation (2) becomes exponentially large. We thus must rely on a diagrammatic expansion of the four-field average to identify the scattering sequences that will contribute the most to the 2p-CBS. This requires great care in the reflection geometry since sequences with few scattering events contribute significantly and a rich variety of diagrams may play a prominent role for strong disorder. With the help of two complementary approaches, one based on a Feynman-path-type decomposition and the other on a random matrix theory formulation, we show that the correlator in equation (2) is dominated by the bi-diffuson and bi-cooperon represented in Fig. 1d, in the regime where the transport mean free path of light, ℓ , exceeds the wavelength λ (see Supplementary Section 6 for details). This correlator is expressed as

$$\Gamma_{ba} = \Gamma_0 \left[1 + F(|\mathbf{q}_a - \mathbf{q}_b|)^2 \right],\tag{5}$$

where Γ_0 is the amplitude of the bi-diffuson and $F(\mathbf{q})$ is a lineshape function between 0 and 1, proportional to the transverse Fourier transform of the diffuse intensity. The latter is a decaying function of range $1/\ell$, indicating that most photons experience a few scattering events before being reflected. Comparing the result for double-passage samples (equation (3)) and for strongly disordered samples (equation (5)), we find that in both cases the width of the CBS peak is inversely proportional to the typical transverse distance between the photons when they exit the medium, $L\theta_0$ for the double-passage configuration and ℓ for strongly disordered samples. It is instructive to compare equation (5) with the mean reflection coefficient $R_{ba} = |r_{\mathbf{q}_b,\mathbf{q}_a}|^2$ that characterizes the classical 1p-CBS. Using the same diagrammatic framework and assuming negligible single-scattering contribution, we obtain

$$R_{ba} = R_0 [1 + F(|\mathbf{q}_a + \mathbf{q}_b|)],$$
 (6)

where R_0 is the amplitude of the diffuson. This means that the contrast of 2p-CBS is simply the square of the contrast of 1p-CBS, in the limit $k\ell \gg 1$ and in the absence of single-scattering contribution in the 1p-CBS. For a semi-infinite disordered medium without absorption, $F(q) \simeq 1 - 2q\ell$ in the vicinity of the backscattering angle q = 0 (ref. 14), so that the 2p-CBS is predicted to be cone shaped, with a width approximately half that of the 1p-CBS cone. Finally, we note that the result in equation (5) is surprisingly different from the total intensity correlation function $\overline{R_bR_a}$, where $R_a = \sum_{a'} |r_{\mathbf{q}_a\mathbf{q}_a'}|^2$, which is known to be dominated by long-range contributions made of pairs of conjugated propagating fields that exchange diffusing partners inside the medium 18,57,58. We show in Supplementary Section 6 that similar long-range contributions occur in the evaluation of Γ_{ba} , but have a relative weight of ~1/ $k\ell$ with respect to the bi-diffuson and bi-cooperon.

To rigorously test these predictions of 2p-CBS in the multiple-scattering regime, we perform numerical simulations that directly solve the scalar wave equation in two dimensions, $[\nabla^2 + k^2 \varepsilon_r(x, y)] \psi(x, y) = 0$, with no approximation beyond spatial discretization. Evaluating the two-photon correlation function through equation (2) requires the full $N \times N$ reflection matrix r for all incoming and outgoing states, averaged over a large number of disorder realizations to suppress speckle fluctuations. The disordered media should have width $W \gtrsim 60\ell$ to resolve the 2p-CBS cone shape, and thickness $L \gg \ell$ to be in the multiple-scattering regime with sufficient long trajectories that contribute to the sharpness of the cone at small angles¹⁵. While full-wave reflection matrix computations of such large systems would normally take a prohibitive amount of computing resources, some of us recently developed a scattering-matrix computation method called augmented partial factorization (APF)⁵⁹ that is many orders of magnitude more efficient. Using APF, we compute 4,000 distinct reflection matrices in plane-wave basis for different disorder realizations, each consisting of 56,000 randomly positioned 0.8λ-diameter dielectric cylinders in air with 10% filling fraction (Fig. 4a). The transport mean free path is $\ell = 9.5\lambda$ (see Methods for details).

Figure 4b shows the numerically calculated 1p-CBS (blue circles) and 2p-CBS (green diamonds) cones; data across the full angular range are shown in Supplementary Fig. 11. We find the peak-to-background ratio of the 1p-CBS cone to be 1.94; the reduction below 2 comes from single scattering in reflection, which does not contribute to the cone^{60,61}. We indeed observe a sharp 2p-CBS cone, validating our analytical prediction. The enhancement factor of the 2p-CBS cone is found to be 2 with no reduction; this is because in the Klyshko's advanced wave picture for two-photon coincidence, photons traverse the system twice so they must be scattered at least twice, with no single-scattering contribution left. The 2p-CBS contrast (green diamonds) is narrower and agrees with the square of the 1p-CBS contrast (orange solid line), in agreement with the analytical prediction above.

To investigate the dependence on the transport mean free path, we vary the filling fraction between 6% and 17%. The full set of 1p-CBS and 2p-CBS data are shown in Supplementary Fig. 12. Figure 4c summarizes the transport mean free path dependence of the numerically computed angular full-width at half-maximum (FWHM) of the 1p-CBS and 2p-CBS cones, which are well described by single-parameter fits of $0.78/(k\ell)$ for 1p-CBS and $0.43/(k\ell)$ for 2p-CBS.

The fact that the 2p-CBS cone has a smaller width and larger slope near the cone's peak suggests that it could yield a better estimate of the transport mean free path than 1p-CBS. To make this intuition quantitative, we evaluated the Cramer–Rao lower bound on the parameter ℓ , which sets a lower bound on the variance of any estimator of ℓ . It is given by the inverse of the Fisher information matrix $\mathcal F$. An important property of 1p-CBS and 2p-CBS is the presence of speckle fluctuations in the CBS map, which add up to the Poisson fluctuations of the detector. Specifically—and this is a key aspect of the following discussion—the statistics of two-photon speckle built with an EPR state made of a large number of modes N is identical to the statistics of one-photon speckle, in sharp contrast with the two-photon speckle of non-entangled states or mixed states²⁶. Taking into account both the speckle and the Poisson noise, we find the elements of the matrix $\mathcal F$ for 2p-CBS to be (Supplementary Section 8)

$$\mathcal{F}_{ij}^{(2p)} = \sum_{h} \frac{N_r}{N_r + N_{ba}} \frac{\partial_{\theta_i} N_{ba} \, \partial_{\theta_j} N_{ba}}{N_{ba}},\tag{7}$$

where $N_{ba} \propto \Gamma_{ba}$ is the number of coincidences detected during the acquisition time, θ_i are the unknown parameters of the problem at hand, N_r is the number of disorder realizations and the sum runs over the independent positions (separated by a distance larger than the angular size of a speckle grain) probed by the detector D_b. Interestingly, in the limit where speckle noise dominates $(N_r \ll N_{ba})$, \mathcal{F}_{ij} becomes independent of the amplitude Γ_0 of the coincidence rate; in particular, in the situation where only ℓ is unknown, we get $\mathcal{F}_{\ell\ell}^{(2p)} = N_r \sum_b (\partial_\ell \Gamma_{ba}/\Gamma_{ba})^2$. Similarly, for 1p-CBS, we find $\mathcal{F}_{\ell\ell}^{(1p)} = N_r \sum_b (\partial_\ell R_{ba}/R_{ba})^2$. With the theoretical $\mathcal{F}_{\ell\ell}^{(1p)} = N_r \sum_b (\partial_\ell R_{ba}/R_{ba})^2$. retical expressions established previously for Γ_{ba} and R_{ba} (see equations (5) and (6)), we immediately conclude that $\mathcal{F}_{\ell\ell}^{(2p)} = 4\mathcal{F}_{\ell\ell}^{(1p)}$ in the vicinity of the cone centre. Remarkably, this result holds independently of the precise expression of the CBS profile F(q), because the 2p-CBS contrast is simply the square of the 1p-CBS contrast. We conclude that the Cramer–Rao lower bound on ℓ is reduced by a factor 4 using 2p-CBS of the EPR state instead of 1p-CBS, in the common situation where Poisson noise is negligible (long integration time).

To summarize, we experimentally observed coherent backscattering of maximally entangled photon pairs from a dynamically changing scattering medium. We provided an in-depth analysis of the fundamental processes governing the phenomenon, revealing unique types of diagrams that determine the scattering process, and which are also absent in classical coherent backscattering. In particular, we find that the two-photon CBS shape is precisely the square of the classical CBS shape in strongly disordered media, as verified by full-wave numerical simulations. Consequently, the Cramer-Rao lower bound for estimating the transport mean free path from the two-photon CBS shape is four times lower than the bound for classical CBS. The narrower CBS shape can be attributed to the fact that correlations between entangled photons mimic propagation of a single photon at half the wavelength. While such wavelength scaling is typically sensitive to dephasing and noise, we find that in two-photon CBS it prevails scattering and disorder averaging. Finally, we note that since both the Klyshko picture provided to understand two-photon CBS and the cooperon object employ the optical reciprocity principle, it would be interesting to study its role in two-photon CBS by utilizing reciprocity breaking techniques44,62.

Online content

Any methods, additional references, Nature Portfolio reporting summaries, source data, extended data, supplementary information, acknowledgements, peer review information; details of author contributions and competing interests; and statements of data and code availability are available at https://doi.org/10.1038/s41567-022-01895-3.

References

- Aspect, A., Dalibard, J. & Roger, G. Experimental test of Bell's inequalities using time-varying analyzers. Phys. Rev. Lett. 49, 1804 (1982).
- Bouwmeester, D. et al. Experimental quantum teleportation. Nature 390, 575–579 (1997).
- 3. Ekert, A. & Renner, R. The ultimate physical limits of privacy. *Nature* **507**, 443–447 (2014).
- Knill, E., Laflamme, R. & Milburn, G. J. A scheme for efficient quantum computation with linear optics. *Nature* 409, 46–52 (2001).
- Yin, J. et al. Satellite-based entanglement distribution over 1200 kilometers. Science 356, 1140–1144 (2017).
- 6. Lum, D. J. et al. Witnessing the survival of time-energy entanglement through biological tissue and scattering media. *Biomed. Opt. Express* **12**, 3658–3670 (2021).
- Candé, M., Goetschy, A. & Skipetrov, S. Transmission of quantum entanglement through a random medium. *Europhys. Lett.* 107, 54004 (2014).
- Valencia, N. H., Goel, S., McCutcheon, W., Defienne, H. & Malik, M. Unscrambling entanglement through a complex medium. *Nat. Phys.* 16, 1112–1116 (2020).
- Pors, B.-J., Monken, C., Eliel, E. R. & Woerdman, J. Transport of orbital-angular-momentum entanglement through a turbulent atmosphere. Opt. Express 19, 6671–6683 (2011).
- Ibrahim, A. H., Roux, F. S., McLaren, M., Konrad, T. & Forbes, A. Orbital-angular-momentum entanglement in turbulence. *Phys. Rev. A* 88, 012312 (2013).
- Krenn, M., Handsteiner, J., Fink, M., Fickler, R. & Zeilinger, A. Twisted photon entanglement through turbulent air across vienna. Proc. Natl Acad. Sci. USA 112, 14197–14201 (2015).
- Leonhard, N. D., Shatokhin, V. N. & Buchleitner, A. Universal entanglement decay of photonic-orbital-angular-momentum qubit states in atmospheric turbulence. *Phys. Rev. A* 91, 012345 (2015).
- Mishchenko, M. I., Travis, L. D. & Lacis, A. A. Multiple Scattering of Light by Particles: Radiative Transfer and Coherent Backscattering (Cambridge Univ. Press, 2006).
- van Rossum, M. C. W. & Nieuwenhuizen, T. M. Multiple scattering of classical waves: microscopy, mesoscopy, and diffusion. *Rev. Mod. Phys.* 71, 313 (1999).
- 15. Akkermans, E. & Montambaux, G. Mesoscopic Physics of Electrons and Photons (Cambridge Univ. Press, 2007).
- 16. Carminati, R. & Schotland, J. C. Principles of Scattering and Transport of Light (Cambridge Univ. Press, 2021).
- Feng, S., Kane, C., Lee, P. A. & Stone, A. D. Correlations and fluctuations of coherent wave transmission through disordered media. *Phys. Rev. Lett.* 61, 834 (1988).
- Mello, P. A., Akkermans, E. & Shapiro, B. Macroscopic approach to correlations in the electronic transmission and reflection from disordered conductors. *Phys. Rev. Lett.* 61, 459 (1988).
- Kuga, Y. & Ishimaru, A. Retroreflectance from a dense distribution of spherical particles. J. Opt. Soc. Am. A 1, 831–835 (1984).
- Van Albada, M. P. & Lagendijk, A. Observation of weak localization of light in a random medium. *Phys. Rev. Lett.* 55, 2692 (1985).
- Wolf, P.-E. & Maret, G. Weak localization and coherent backscattering of photons in disordered media. *Phys. Rev. Lett.* 55, 2696 (1985).
- Akkermans, E., Wolf, P. & Maynard, R. Coherent backscattering of light by disordered media: analysis of the peak line shape. *Phys. Rev. Lett.* 56, 1471 (1986).
- Crespi, A. et al. Anderson localization of entangled photons in an integrated quantum walk. *Nat. Photonics* 7, 322–328 (2013).

- Di Giuseppe, G. et al. Einstein-podolsky-rosen spatial entanglement in ordered and anderson photonic lattices. *Phys. Rev. Lett.* 110, 150503 (2013).
- Gilead, Y., Verbin, M. & Silberberg, Y. Ensemble-averaged quantum correlations between path-entangled photons undergoing anderson localization. *Phys. Rev. Lett.* 115, 133602 (2015).
- Beenakker, C., Venderbos, J. & Van Exter, M. Two-photon speckle as a probe of multi-dimensional entanglement. *Phys. Rev. Lett.* 102, 193601 (2009).
- Ott, J. R., Mortensen, N. A. & Lodahl, P. Quantum interference and entanglement induced by multiple scattering of light. *Phys. Rev.* Lett. 105, 090501 (2010).
- 28. Candé, M. & Skipetrov, S. E. Quantum versus classical effects in two-photon speckle patterns. *Phys. Rev. A* **87**, 013846 (2013).
- Schotland, J. C., Cazé, A. & Norris, T. B. Scattering of entangled two-photon states. Opt. Lett. 41, 444–447 (2016).
- Lodahl, P. & Lagendijk, A. Transport of quantum noise through random media. Phys. Rev. Lett. 94, 153905 (2005).
- 31. Lodahl, P., Mosk, A. & Lagendijk, A. Spatial quantum correlations in multiple scattered light. *Phys. Rev. Lett.* **95**, 173901 (2005).
- Smolka, S., Huck, A., Andersen, U. L., Lagendijk, A. & Lodahl, P. Observation of spatial quantum correlations induced by multiple scattering of nonclassical light. *Phys. Rev. Lett.* 102, 193901 (2009).
- Smolka, S., Ott, J. R., Huck, A., Andersen, U. L. & Lodahl, P. Continuous-wave spatial quantum correlations of light induced by multiple scattering. *Phys. Rev. A* 86, 033814 (2012).
- 34. Peeters, W., Moerman, J. & Van Exter, M. Observation of two-photon speckle patterns. *Phys. Rev. Lett.* **104**, 173601 (2010).
- Di Lorenzo Pires, H., Woudenberg, J. & van Exter, M. P. Statistical properties of two-photon speckles. *Phys. Rev. A* 85, 033807 (2012).
- van Exter, M. P., Woudenberg, J., Di Lorenzo Pires, H. & Peeters, W. H. Bosonic, fermionic, and anyonic symmetry in two-photon random scattering. *Phys. Rev. A* 85, 033823 (2012).
- Defienne, H., Reichert, M. & Fleischer, J. W. Adaptive quantum optics with spatially entangled photon pairs. *Phys. Rev. Lett.* 121, 233601 (2018).
- 38. Jakeman, E. Enhanced backscattering through a deep random phase screen. *J. Opt. Soc. Am. A* **5**, 1638–1648 (1988).
- Dogariu, A., Boreman, G. D. & Dogariu, M. Enhanced backscattering from a volume-scattering medium behind a phase screen. Opt. Lett. 20, 1665–1667 (1995).
- Schwartz, C. & Dogariu, A. Enhanced backscattering of optical vortex fields. Opt. Lett. 30, 1431–1433 (2005).
- Wiersma, D. S., van Albada, M. P. & Lagendijk, A. Coherent backscattering of light from amplifying random media. *Phys. Rev. Lett.* 75, 1739 (1995).
- Yoo, K., Tang, G. & Alfano, R. Coherent backscattering of light from biological tissues. Appl. Optics 29, 3237–3239 (1990).
- 43. Derode, A., Mamou, V., Padilla, F., Jenson, F. & Laugier, P. Dynamic coherent backscattering in a heterogeneous absorbing medium: application to human trabecular bone characterization. *Appl. Phys. Lett.* **87**, 114101 (2005).
- 44. Bromberg, Y., Redding, B., Popoff, S. & Cao, H. Control of coherent backscattering by breaking optical reciprocity. *Phys. Rev. A* **93**, 023826 (2016).

- 45. Labeyrie, G. et al. Coherent backscattering of light by cold atoms. *Phys. Rev. Lett.* **83**, 5266 (1999).
- 46. Huang, J. et al. Anomalous coherent backscattering of light from opal photonic crystals. *Phys. Rev. Lett.* **86**, 4815 (2001).
- Scalia, P. S., Muskens, O. L. & Lagendijk, A. Weak localization of photon noise. New J. Phys. 15, 105009 (2013).
- 48. Fazio, B. et al. Coherent backscattering of Raman light. *Nat. Photonics* **11**, 170–176 (2017).
- 49. Bayer, G. & Niederdränk, T. Weak localization of acoustic waves in strongly scattering media. *Phys. Rev. Lett.* **70**, 3884 (1993).
- Larose, E., Margerin, L., Van Tiggelen, B. & Campillo, M. Weak localization of seismic waves. *Phys. Rev. Lett.* 93, 048501 (2004).
- 51. Jendrzejewski, F. et al. Coherent backscattering of ultracold atoms. *Phys. Rev. Lett.* **109**, 195302 (2012).
- 52. Potton, R. J. Reciprocity in optics. Rep. Prog. Phys. 67, 717 (2004).
- 53. Belinskii, A. & Klyshko, D. Two-photon optics: diffraction, holography, and transformation of two-dimensional signals. *J. Exp. Theor. Phys.* **78**, 259–262 (1994).
- 54. Walborn, S., Monken, C., Pádua, S. & Souto Ribeiro, P. Spatial correlations in parametric down-conversion. *Phys. Rep.* **495**, 87–139 (2010).
- 55. Smolka, S. Quantum Correlations and Light Localization in Disordered Nanophotonic Structures. PhD thesis, Technical Univ. Denmark (2010).
- 56. Boto, A. N. et al. Quantum interferometric optical lithography: exploiting entanglement to beat the diffraction limit. *Phys. Rev. Lett.* **85**, 2733 (2000).
- 57. Rogozkin, D. B. & Cherkasov, M. Y. Long-range intensity correlations in wave reflection from a disordered medium. *Phys. Rev. B* **51**, 12256 (1995).
- Hsu, C. W., Goetschy, A., Bromberg, Y., Stone, A. D. & Cao, H. Broadband coherent enhancement of transmission and absorption in disordered media. *Phys. Rev. Lett.* 115, 223901 (2015).
- Lin, HC., Wang, Z. & Hsu, C.W. Fast multi-source nanophotonic simulations using augmented partial factorization. *Nat. Comput.* Sci. 2, 815–822 (2022).
- 60. van Tiggelen, B. A., Wiersma, D. A. & Lagendijk, A. Self-consistent theory for the enhancement factor in coherent backscattering. *Europhys. Lett.* **30**, 1 (1995).
- 61. Amic, E., Luck, J. M. & Nieuwenhuizen, T. M. Anisotropic multiple scattering in diffusive media. *J. Phys. A* **29**, 4915 (1996).
- Muskens, O. L., Venn, P., van der Beek, T. & Wellens, T.
 Partial nonlinear reciprocity breaking through ultrafast
 dynamics in a random photonic medium. *Phys. Rev. Lett.* 108,
 223906 (2012).

Publisher's note Springer Nature remains neutral with regard to jurisdictional claims in published maps and institutional affiliations.

Springer Nature or its licensor (e.g. a society or other partner) holds exclusive rights to this article under a publishing agreement with the author(s) or other rightsholder(s); author self-archiving of the accepted manuscript version of this article is solely governed by the terms of such publishing agreement and applicable law.

© The Author(s), under exclusive licence to Springer Nature Limited 2023

Methods

Experiment

We used a CW laser at $\lambda_p = 404$ nm (OBIS, Coherent) to pump a h = 2 mm long periodically poled potassium titanyl phosphate (PPKTP) crystal in a collinear type 0 degenerate configuration. Pairs of degenerate entangled photons (signal and idler) at $\lambda = 808$ nm were thus generated via SPDC. The beam waist at the incidence plane of the crystal was approximately $w_p = 550 \mu m$, yielding spatially entangled photons with a Schmidt number of $K = \frac{k_p w_p^2}{4h} \approx 588 \text{ (ref. 63)}$. The remainder of the pump beam is deflected via a dichroic mirror located right after the crystal. The down-converted photons were selected via interference filters at $\lambda = 809 \pm 40$ nm. In the 2p-CBS experiment, both photons were imaged to a spot area of approximately 1 mm² via a 4f system (f = 150 mm) on a polarization-preserving diffuser of 1 inch diameter (Luminit, circular Light Shaping Diffusers), behind which a plane mirror was placed. Dynamic scattering was achieved by rotating the diffuser at approximately 5,300 rounds per minute using a custom-built rotation stage and simultaneously translating the diffuser in the transverse horizontal direction at a speed of 2 mm s⁻¹. The entire area of the diffuser was therefore covered by the SPDC spot within 6 seconds, corresponding to over 500 disorder realizations that change at an average rate of approximately 80 realizations per second. The measured scattering angle of the diffuser, defined by the 1/e width of its disorder-averaged far-field intensity distribution (see equation (4.3) of Supplementary Section 4), was measured to be $\theta_0 \approx 4.4$ mrad. The reflected light was then scattered once more off the rotating diffuser, and collected by a lens ($f_4 = 200 \text{ mm}$) and two fibre-coupled single-photon detectors (Excelitas SPCM-AQ4C) of radius σ = 50 μ m located at the Fourier plane of the diffuser. The coincidence circuit was implemented using Swabian Instruments' Time Tagger 20 with a temporal coincidence window of 800 ps. The figures in this article presenting the coincidence count rates are corrected for the accidental coincidence counts. In the 1p-CBS experiment, the idler photon was detected with a lens ($f_1 = 150$ mm) and a stationary fibre-coupled detector located at the Fourier plane of the crystal, whereas the signal photon was directed into the circuit mentioned above. The number of modes in our experiment, N, is smaller than the Schmidt number K by a factor of approximately 5, given by the square of the ratio of the SPDC divergence angle (\$\approx 20 \text{ mrad}) and the scattering angle of the diffuser θ_0 . For a more detailed description of the experimental setup, see Supplementary Section 1.

Numerical simulations

Numerical simulations were performed by solving the scalar wave equation in two dimensions, $[\nabla^2 + k^2 \varepsilon_r(x,y)] \psi(x,y) = 0$, using finite-difference discretization with grid resolution $\Delta x = \lambda/10$ and subpixel smoothing⁶⁴. Each disordered medium consists of 56,000 randomly positioned dielectric cylinders with refractive index n = 1.5 and diameter $2r_0 = 0.8\lambda$ in air, inside a region with width $W = 700\lambda$ and varying thickness L. Periodic boundary condition was used in the direction along W to mimic an infinite system, so the angle is discretized at a resolution $\delta\theta = \lambda/W$ at small angles. Perfectly matched layer⁶⁵ was used in the direction along L to implement an outgoing boundary. Note that since the 2p-CBS cone has an angular full-width at half-maximum of $0.43/(k\ell)$, a system width of $W > 4\lambda/\text{FWHM} \approx 58\ell$ is needed to resolve five or more angles with $\delta\theta$ spacing within the half-maximum of the 2p-CBS cone. Here, an individual dielectric cylinder has a scattering cross-section $\sigma_{sca} = 3.02\lambda$ and an anisotropy factor $g \equiv \langle \cos \theta \rangle = 0.825$, obtained from its differential scattering cross-section numerically computed by near-to-far-field transformation for such cylinders at $\Delta x = \lambda/10$. We obtained the transport mean free path directly through the independent-particle approximation as $\ell = [\sigma_{sca}\rho(1-g)]^{-1}$, where ρ is the number density. To vary ℓ , the thickness L of the scattering region was varied between $L = 232\lambda$ and $L = 695\lambda$ while fixing width W and the number of dielectric cylinders (corresponding to filling fraction $\pi r_0^2 \rho$ between 17% and 5.8%); the numerically computed average transmission \bar{T} stays between 3.7% and 3.8% for different L, in excellent agreement with the analytic prediction of $\bar{T} = [1 + (2/\pi)(L/\ell)]^{-1} = 3.6\%$ (ref. 66), indicating the ℓ computed from independent-particle approximation is accurate for these configurations. We used the full-wave method APF⁵⁹ to compute the complete $2N \times 2N$ scattering matrix (which includes the reflection matrices from both sides) without looping over the input states, with $N = 1,425 \approx 2W/\lambda$ being the number of propagating plane-wave channels on one side. We performed the simulations for 2,000 realizations of disorder at each L, giving 4,000 reflection matrices per thickness. To further suppress the speckle fluctuations, we also averaged over 29 vertical slices of matrix $|r_{q_0,q_0}|^2$ and $|(r^2)_{\mathbf{q}_b,-\mathbf{q}_a}|^2$ centred within ± 20 mrad from $\mathbf{q}_a = 0$ while excluding \mathbf{q}_b at the exact specular direction. The computations were done on the USC Center for Advanced Research Computing's Discovery cluster.

Data availability

Source data are provided with this paper. All other data that support the plots within this paper and other findings of this study are available from the corresponding author upon reasonable request.

Code availability

Simulations performed in this work use the augmented partial factorization method implemented in software MESTI, available at https://github.com/complexphoton/MESTI.m.

References

- 63. Law, C. & Eberly, J. Analysis and interpretation of high transverse entanglement in optical parametric down conversion. *Phys. Rev. Lett.* **92**, 127903 (2004).
- Farjadpour, A. et al. Improving accuracy by subpixel smoothing in the finite-difference time domain. Opt. Lett. 31, 2972–2974 (2006).
- 65. Gedney, S. in Computational Electrodynamics: The Finite-Difference Time-Domain Method 3rd edn (eds Taflove, A. & Hagness, S. C.) Ch. 7 (Artech House, 2005).
- 66. Beenakker, C. W. J. Random-matrix theory of quantum transport. *Rev. Mod. Phys.* **69**, 731 (1997).

Acknowledgements

Funding: Zuckerman STEM Leadership Program, the Israel Science Foundation (grant no. 2497/21), National Science Foundation (ECCS-2146021), LABEX WIFI (Laboratory of Excellence within the French Program 'Investments for the Future') under references ANR-10-LABX-24 and ANR-10-IDEX-0001-02 PSL*.

Author contributions

M.S., O.L. and Y.B. conceived the idea and designed the experiments. M.S. built the experimental setup, performed the measurements and developed the theory for the double-passage configuration. A.G. developed the theory in the multiple-scattering regime and Fisher information analysis. H.-C.L. and C.W.H. performed the numerical simulations. All authors analysed the results and contributed to the manuscript preparation.

Competing interests

The authors declare no competing interests.

Additional information

Supplementary information The online version contains supplementary material available at https://doi.org/10.1038/s41567-022-01895-3.

 $\begin{tabular}{ll} \textbf{Correspondence and requests for materials} should be addressed to Yaron Bromberg. \end{tabular}$

Peer review information *Nature Physics* thanks Mauro Paternostro, Bienvenu Ndagano and the other, anonymous,

reviewer(s) for their contribution to the peer review of this work.

Reprints and permissions information is available at www.nature.com/reprints.